Characterization of ^{1}H NMR Signal in Human Cortical Bone for Magnetic Resonance Imaging

R. Adam Horch,[1,2] Jeffry S. Nyman,[3,4] Daniel F. Gochberg,[2,5] Richard D. Dortch,[2,5] and Mark D. Does[1,2,5,6]*

Recent advancements in MRI have enabled clinical imaging of human cortical bone, providing a potentially powerful new means for assessing bone health with molecular-scale sensitivities unavailable to conventional X-ray-based diagnostics. In human cortical bone, MRI is sensitive to populations of protons (^{1}H) partitioned among water and protein sources, which may be differentiated according to intrinsic NMR properties such as chemical shift and transverse and longitudinal relaxation rates. Herein, these NMR properties were assessed in human cortical bone donors from a broad age range, and four distinct ^{1}H populations were consistently identified and attributed to five microanatomical sources. These findings show that modern human cortical bone MRI contrast will be dominated by collagen-bound water, which can also be exploited to study human cortical bone collagen via magnetization transfer. Magn Reson Med 64:680–687, 2010. © 2010 Wiley-Liss, Inc.

Key words: NMR; MRI; relaxometry; bone collagen; bone water; bone pore

As the skeleton ages, the risk of fracture increases. This increasing propensity to fracture is not solely due to the well-documented loss of bone mass with aging but also to a deterioration in strength and toughness of bone (bone quality) (1). Clinical measurements of bone mass by gold-standard dual-energy X-ray absorptiometry are relatively insensitive to soft tissue characteristics in bone such as water molecule distribution, which has been conclusively linked to the energy dissipation mechanisms of the bone matrix (2–8) and likely plays a pivotal role in bone quality. Unlike X-ray-based imaging modalities, MRI is highly sensitive to the water microenvironment in tissue, as well as other molecular sources of ^{1}H, and offers the potential to noninvasively evaluate bone

quality. While conventional MRI methods are not suitable for imaging cortical bone because of its low proton density and short T_2 constants, so-called ultrashort echo time and related MRI methods have opened clinical MRI to hard tissue imaging (9–11). Recently, these methods have produced high-quality images of human cortical bone (HCB) (10,12) and raised the question of what bone characteristics can be derived from such images. Presented herein is a phenomenological and biophysical characterization of the ultrashort echo time MRI-visible ^{1}H NMR signal of HCB. Specifically, unique contributions to the net HCB NMR signal are determined for both bound and mobile water, lipids, and bone matrix collagen. Knowledge of these signal contributions and their NMR properties is critical for future development and interpretation of cortical bone MRI and may form the foundation for a novel diagnostic of bone health.

Cortical bone is a complex composite of nano- and microstructural components, including type-I collagen, calcium phosphate mineral deposits, interosteonal lipids, and porous spaces such as haversian canals and the lacunar-canalicular system, which generally occur in repeating units of osteons (Fig. 1) (13–15). It is likely that each of these tissue components includes one or more distinct proton microenvironments, which differ according to their local chemical, magnetic, and electrical milieu. For example, the collagen component is host to both macromolecular-adsorbed water and covalently bound backbone protons, while mineral and porous spaces contain water with varying degrees of motional restriction, and lipids can be found in the cement line spaces between osteons (14). These proton microenvironments are too small to be spatially resolved with clinical MRI, but their ^{1}H NMR signal contributions may be resolved by decomposing the net NMR signal into chemical shift and relaxation components. Presented here is a series of NMR measurements at 4.7 T, relevant signal decompositions, and physical manipulations of HCB specimens from cadaveric donors to identify common signal components and their microanatomic origins.

MATERIALS AND METHODS

HCB Preparation

The Musculoskeletal Tissue Foundation (Edison, NJ), a nonprofit tissue allograft bank, and the Vanderbilt Donor Program (Nashville, TN) supplied human femurs from six cadaveric donors (four male, two female, aged 21–94 years old, mean ± standard deviation: 60 ± 31 years)

[1]Department of Biomedical Engineering, Vanderbilt University, Nashville, Tennessee, USA.

[2]Institute of Imaging Science, Vanderbilt University, Nashville, Tennessee, USA.

[3]VA Tennessee Valley Healthcare System, Vanderbilt University, Nashville, Tennessee, USA.

[4]Orthopaedics & Rehabilitation Medicine, Vanderbilt University, Nashville, Tennessee, USA.

[5]Radiology and Radiological Sciences, Vanderbilt University, Nashville, Tennessee, USA.

[6]Electrical Engineering, Vanderbilt University, Nashville, Tennessee, USA.

*Correspondence to: Mark D. Does, Ph.D., Vanderbilt University Institute of Imaging Science, 1161 21st Ave South, AA-1105, Nashville, TN 37232-2310. E-mail: mark.does@vanderbilt.edu
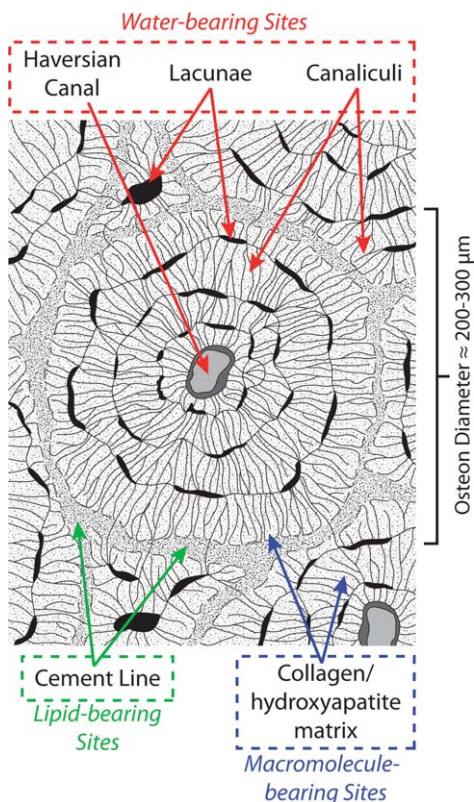
FIG. 1. Bone matrix schematic. Expected biophysical distribution of osteonal water, lipid, and macromolecule-bearing proton sites in HCB are identified in red, green, and blue, respectively. The primary nano- and microstructures housing each of these sites are given in dashed boxes.

under instruction to not provide tissue from donors who had tested positive for a blood-borne pathogen (e.g., human immunodeficiency virus or hepatitis C). One HCB specimen was extracted from the medial midshaft of each donor's right femur and was machined to 15 × 5 × 5 mm dimensions via end mill. During dimensioning, care was taken to remove endosteal and periosteal surfaces such that the final specimens for NMR measurement were pure cortical bone. Specimens were stored in phosphate-buffered saline at −20°C between processing and NMR measurements, and specimens were thawed at 4°C approximately 18 h prior to NMR measurements. Immediately prior to NMR measurements, thawed specimens were removed from phosphate-buffered saline and blotted dry to remove the large amount of pooled surface water that remained. Specimens endured no more than three freeze-thaw cycles, and separate experiments found that up to six freeze-thaw cycles had negligible impact on the NMR properties. Final HCB dimensions were measured with digital caliper for volume determination.

μCT

μCT was performed on 2 × 4 × 4 mm HCB specimens (harvested adjacent to NMR specimen femoral sites) with a Scanco μCT 40 scanner (Scanco Medical, Brüttisellen, Switzerland) at 6-μm isotropic resolution, which was sufficient to image the Haversian canal and vascular po-

rosity. The osteons of the cortical specimen were aligned with the scanning axis using the standard tube. At a resolution of 6-μm voxel size (isotropic), a portion of each specimen (2.4 mm in length) was scanned, acquiring 1000 projections per 180°. X-ray source settings did not vary among the specimens. After reconstruction, the Scanco thresholding procedure segmented bone tissue from air or soft tissue. Applying the Scanco evaluation software to the cortical bone, we quantified porosity, defined as one minus cortical bone volume per total volume.

NMR Measurements

The HCB specimens were initially assessed with measurements of their ^{1}H NMR resonance spectra and T_2 decays, probing NMR signal decay features that dominate ultrashort echo time MRI contrast. NMR measurements were performed in a Varian 4.7-T horizontal-bore magnet with a direct drive receiver (Varian Medical Systems, Palo Alto, CA). An in-house loop-gap style radiofrequency coil was used with Teflon structural support, which gave negligible background ^{1}H signal ($\approx$1% of net HCB signal). Pulse sequences used 90° excitation pulses of $\approx$8-μs duration and (where relevant) 180° refocusing/inversion pulses of $\approx$16-μs duration. Free induction decays (FIDs) were collected at 5-MHz bandwidth and 20-Hz nominal spectral resolution from a pulse-acquire sequence, with an 8-μs dead time after excitation to allow for coil ringing to subside. Four excitations were averaged, using a cyclops phase-cycling scheme. Resonance spectra were calculated from FIDs by discrete Fourier transform and manual phasing. To characterize T_2, Carr-Purcell-Meiboom-Gill (CPMG) (16) measurements with a total of 10,000 echoes were collected at 100-μs echo spacing (first echo at echo time = 100 μs), yielding data that were fitted with a T_2 spectrum (details below). Four excitations were averaged using a $90_{(x,-x,x,-x)}$/$180_{(y,y,-y,-y)}$ phase cycling scheme. Echo spacing was minimized while avoiding spin locking effects, which manifested as prolonged apparent T_2s when echo spacing was <100 μs. In all measurements, HCB specimens were placed with osteonal direction orthogonal to the static field to avoid altering any potential magic angle effects across measurements.

Further investigation of both the FID and CPMG signal included three additional NMR studies: (1) inversion-recovery-prepared CPMG (IR-CPMG), (2) T_2-T_2 relaxation exchange spectroscopy (REXSY) (17), and (3) dynamic study of FID and CPMG signal responses to deuterium oxide (D_2O) immersion. The IR-CPMG measurements involved an IR preparation with variable recovery time preceding a CPMG acquisition, as described above. Twenty-four recovery times, log-spaced between 1 ms and 10 sec, were used for each sample and the resulting data were fitted with a two-dimensional T_1-T_2 spectrum (18) (details below). The REXSY measurements involved a CPMG-like preparation with variable number of echoes, followed by a storage/mixing period then a CPMG acquisition, as described above. Thirty-two different CPMG preparations were used, with echo spacing of 100 μs and number of echoes pseudo-log spaced between 1 and
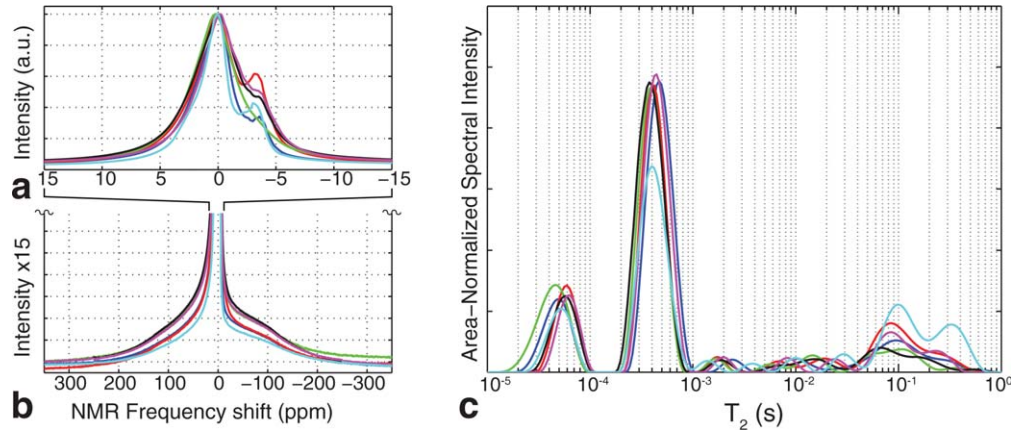
FIG. 2. Wide-line NMR and multiexponential T_2 spectroscopy of HCB specimens. NMR spectroscopy of HCB specimens over narrow **(a)** and broad **(b)** bandwidths generally showed three frequency components in all samples: an off-resonant, narrow-band frequency component at -4.0 ± 0.2 ppm (fat shifted) and on-resonant narrow-band and broadband components. Spectra in **(b)** are magnified 15-fold in the vertical axis of **(a)** and are vertically cropped for display purposes. Multiexponential T_2 spectroscopy of HCB **(c)** reveals two well-defined T_2 pools at 57 ± 4 μs and 416 ± 35 μs and a broad distribution of T_2 components spanning 1 ms to 1000 ms. All spectra were normalized to maximum intensity **(a,b)** or total integrated area **(c)**.

1000. For all acquisitions, the mixing period was 200 ms, and the resulting data were fitted with a T_2-T_2 spectrum. REXSY measurements used an additional phase cycle of the storage pulse (to store T_2-prepared magnetization on the $\pm$ z axis during the mixing period), resulting in a total of four averaged excitations. (For further details on using REXSY for exchange measurements see Dortch et al. (19)). Finally, after all aforementioned NMR measurements, specimens were placed in an isotonic D_2O solution to study effects of proton-deuteron exchange on NMR properties for determination of proton origins. This solution was made by mixing a volume of 99.9% isotopic purity D_2O (Sigma-Aldrich Corp., St. Louis, MO) with the appropriate mass of phosphate-buffered saline electrolyte tablets (MP Biomedicals, Solon, OH) to yield $1\times$ phosphate-buffered saline. Each bone specimen was immersed in a volume of isotonic phosphate-buffered saline that was $100\times$ larger than the specimen volume, and immersed specimens were maintained on a shaker table at 60 revolutions per minute and $4°C$ until steady state was achieved (as determined by monitoring NMR resonance spectra). Final NMR measurements were then collected for comparison to initial measurements.

NMR Data Fitting

After phasing, real-valued NMR resonance spectra were fitted to a sum of three Lorentzian line shapes with a constrained Levenberg-Marquardt algorithm. For each spectrum, visual inspection provided initial guesses of line widths and frequency offsets so as to improve algorithm convergence, and final inspections of residuals and mean square errors verified proper fitting.

The 10,000 CPMG echo magnitudes were downsampled in a pseudo-log fashion to 1024 echoes and fitted to a sum of 128 decaying exponential functions (with time constants log-spaced between 20 μs and 10 sec) in a nonnegative least-squares sense, subject to a minimum curvature constraint, which produced a so-called T_2

spectrum (20). IR-CPMG data were reduced by singular-value decomposition (21) prior to two-dimensional nonnegative least-squares fitting (18) to the aforementioned range of decaying exponentials, producing a so-called T_1-T_2 spectrum. REXSY data were processed in a similar manner, yielding T_2-T_2 spectra. All data processing was performed with MATLAB (The MathWorks, Natick, MA). Results are presented as mean $\pm$ 1 standard deviation across samples.

In order to quantitatively compare the absolute signal amplitudes of T_2 spectra across specimens and days, a 20-μL H_2O reference sample with long T_2 (≈ 2.5 sec) was included in each CPMG measurement. This reference sample, together with its known molar ^1H density and the known HCB specimen volumes, enabled the calculation of proton concentrations in the bulk bone specimens for each CPMG relaxation component by comparing integrated areas of each T_2 spectral component to the area of the marker. No such reference was used during resonance spectrum measurements, but the intermeasurement standard deviation of the reference sample's signal intensity was 4.8%, so it was concluded that the absolute amplitudes of the resonance spectral components were reliable to approximately this degree of precision.

RESULTS

FID-derived NMR resonance spectra (Fig. 2a,b) revealed three distinct signal components, as determined by Lorentzian fitting: two relatively narrow-band, slow-relaxing chemically shifted components were consistently observed atop a broadband, fast-relaxing component. In all specimens, the narrow-band component line widths were <5 parts per million (ppm) and the broad-band component line widths were >100 ppm, giving clear discrimination between slow- and fast-relaxing species. The dominant narrow-band component accounted for 57.7 $\pm$ 3.9% of the total FID signal. The second narrow-band component was consistently chemically shifted from the first component by -4.0 ± 0.2 ppm and represented 4.6
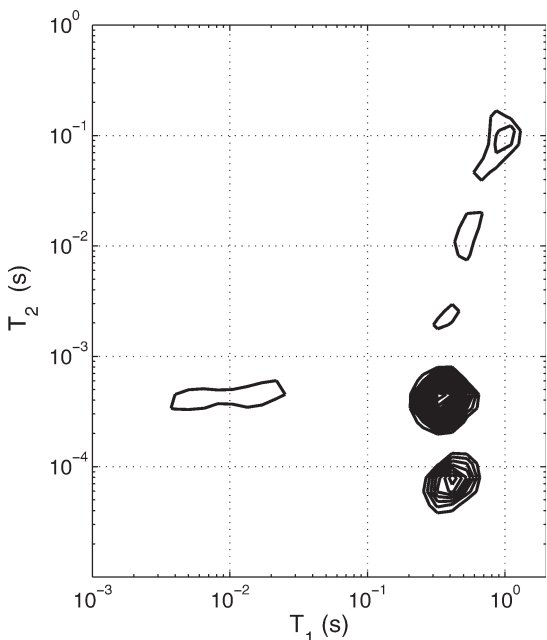
FIG. 3. Two-dimensional T_1-T_2 spectra. Typical results from IR-CPMG data are shown, wherein the T_1 relaxation time(s) for each T_2 component may be identified after a two-dimensional inverse Laplace transform. Note that all T_2 components are monoexponential in T_1 except for the 400-μs T_2, which results from magnetization transfer with a shorter-lived T_2 component.

$\pm$ 3.2% of the FID signal. The broadband component accounted for the remaining 33.7 $\pm$ 2.5% of the FID signal and had a -33 ± 6.8 ppm chemical shift from the dominant narrow-band component. T_2^*s of 736 $\pm$ 46 μs, 1700 $\pm$ 470 μs, and 11.8 $\pm$ 1.1 μs for the on-resonant narrow-band, off-resonant narrow-band, and broadband components, respectively, were calculated from the components' line widths.

Figure 2c shows CPMG-derived T_2 spectra from each HCB specimen, demonstrating two distinct submillisecond relaxation components and a broad collection of signals spanning the millisecond-second T_2 domain, which hereafter is collectively considered a third T_2 component for discussion purposes. The two submillisecond components had T_2s of 57 $\pm$ 4 μs and 416 $\pm$ 35 μs, with respective CPMG bone signal fractions of 16.1 $\pm$ 1.3% and 60.8 $\pm$ 5.3%. The long-lived third T_2 component accounted for the remaining 23.0 $\pm$ 6.5% of the CPMG signal. Comparing these signal fractions to the concomitantly measured T_2 marker (see NMR Data Fitting) gave proton concentrations of 6.6 $\pm$ 1.5, 24.8 $\pm$ 5.8, and 9.2 $\pm$ 2.3 mol ^{1}H/L$_{bone}$ for the $\approx$60-μs, $\approx$400-μs, and long-lived T_2 components, respectively. Note that typical CPMG data signal-to-noise ratio was $\approx$7000 (integrated spectral area divided by the standard deviation of the residuals from the T_2 spectrum fit), which was ample to fit the observed 60-μs T_2 component. In preliminary studies, general characteristics of both resonance and T_2 spectra did not change substantially between 0.5 T and 9.4 T static magnetic field strengths (data not shown), so the three FID and three CPMG signal components should be

relevant to all mainstream laboratory and clinical HCB NMR.

For all HCB specimens, T_1-T_2 spectra from IR-CPMG measurements (Fig. 3) showed T_1 values ranging from $\approx$350 ms for the two short-lived T_2 components to $\approx$1 sec for much of the long-lived T_2 component. A biexponential T_1 relaxation for the $\approx$400 μs T_2 component was consistently observed, characteristic of magnetization transfer between this component and a shorter-T_2 proton pool (22). Observable T_2 proton pools participating in this magnetization transfer were identified from REXSY T_2-T_2 spectra (Fig. 4). The main diagonal in the T_2-T_2 spectrum is analogous to the one-dimensional CPMG-derived T_2 spectrum, while off-diagonal signals arise from an exchange of magnetization between T_2 components during the 200-ms mixing period (similar to EXSY experiments in chemical-shift-resolved studies (23)). As such, REXSY consistently indicated exchange between the two short-lived T_2 components ($\approx$60 μs and $\approx$400 μs). No significant exchange involving the long-lived T_2 signals was observed in any of the HCB samples.

Resonance and T_2 spectra from a representative HCB specimen undergoing prolonged D_2O immersion are shown in Fig. 5a,b. Since the D_2O deuteron is undetectable in ^{1}H NMR measurements and may freely exchange with various protons in bone, these spectra demonstrate a combination of ^{1}H signal components that wash out with D_2O (i.e., water and chemically exchangeable protons such as amines and hydroxyls) and those that do not (methylene protons). Of the three resonance spectra components, the dominant on-resonant narrow-band component was the only component that was nearly
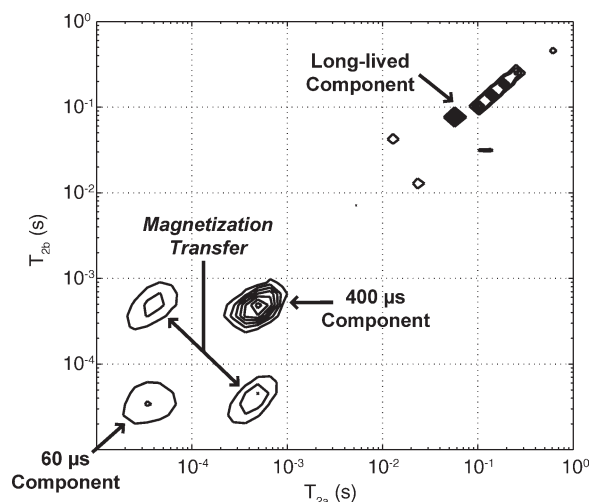

FIG. 4. Two-dimensional REXSY representative of all HCB specimens. Each of the three T_2 components appears on the main diagonal (running lower-left to upper-right), which represents stationary nuclear spins that do not transit between pools during the 200-ms REXSY mixing period and thus maintain a fixed T_2. Off-diagonal cross peaks, observed between the two short-lived T_2 components, indicate spins that exchange via magnetization transfer mechanisms. Thus, the protons relaxing with $T_2 \approx$60 μs and $\approx$400 μs are in molecular contact during the mixing period but effectively remain isolated from the long-lived protons.
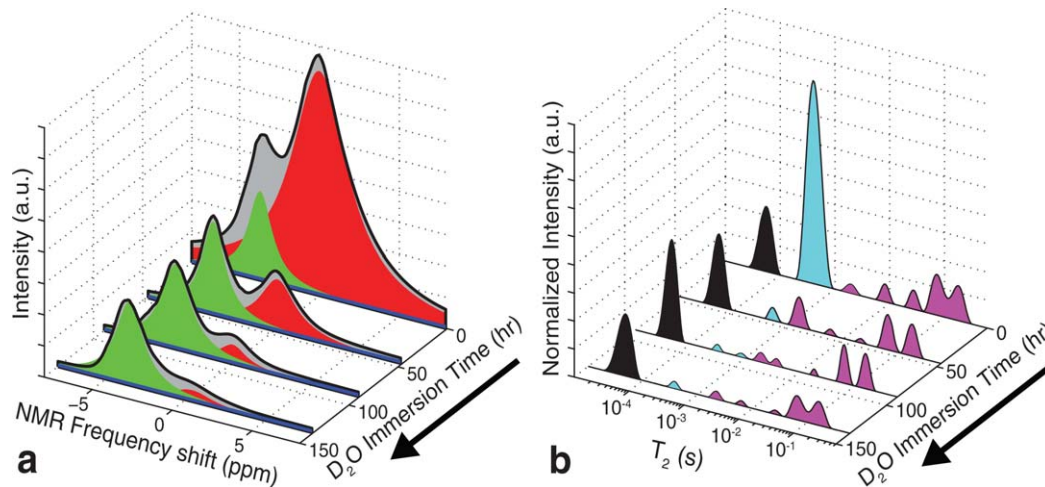
FIG. 5. Effects of D_2O immersion on resonance and multiexponential T_2 spectra of HCB specimens. Resonance **(a)** and T_2 spectra **(b)** are shown at various time points for one representative HCB specimen undergoing D_2O immersion. Resonance spectra, shown in gray and black, were fitted to the sum of three Lorentzian components, which are overlaid in red, blue, and green. T_2 spectra are divided into $\approx$60-μs (black), $\approx$400-μs (cyan), and long-lived (magenta) components for comparison to the three resonant components.

completely washed out (>95%). The off-resonant narrow-band component was unaffected by D_2O immersion, as was 83 $\pm$ 2% of the broadband component (17 $\pm$ 2% washed out). Likewise, the only T_2 component effectively removed by D_2O was the $\approx$400 μs T_2 (>98% washed out). The $\approx$60-μs T_2 component was unaffected by D_2O immersion (to within the tolerances associated with CPMG data fitting), and 58 $\pm$ 12% of the long-lived T_2 component was removed by D_2O.

DISCUSSION

In animal (24–26) or human (27–31) cortical bones, previous studies have identified various subsets of the six NMR components observed herein but have not entirely agreed upon or thoroughly explored their biophysical origins. In particular, the large, submillisecond T_2 component has been attributed to both macromolecular-bound water (25,27–31) and porous water of the lacunae and canaliculi (12,26). Because this signal will dominate most standard ultrashort echo time MRI scans of cortical bone, understanding its biophysical origin and relation to all other signal components is important for interpreting cortical bone MRI. By comparing results from our combination of studies, we have reasoned the biophysical origins of all the FID and CPMG signal components. These assignments and relevant data are summarized in Fig. 6 and the rationale is outlined as follows.

Based on its chemical shift, endurance through D_2O immersion, and relatively slow relaxation rate, the off-resonant FID component must arise from mobile methylene protons—most likely found on lipids (as similarly concluded by Fernandez-Seara et al. (6)). The line width of this component ($\approx$1 ppm) corresponds to a $T_2^* \approx$1.6 ms; therefore, it must be present as a fraction of the long-T_2 component ($\approx$45%) that also survives D_2O immersion. Aside from the lipid signal, most of the remaining signal that survives D_2O immersion—the broadband FID and short-lived CPMG components—

must, by nature of their very short T_2/T_2^* signals, be derived from relatively immobile methylene protons. The majority of these protons must belong to collagen macromolecules, which represent >90% of the organic mass in HCB (15). Note that both the broadband FID and short-lived CPMG components may arise from the same collagen molecules, but they likely do not originate from the same protons due to the $\approx$70,000 sec^{-1} difference in their relaxation rates ($1/T_2^*$ and $1/T_2$), which is too large to be entirely caused by static magnetic field variations and must arise from different molecular dynamics. It is conceivable that the faster-relaxing FID broadband protons occupy methylene sites on the semicrystalline collagen triple helix backbone, while the slower-relaxing $\approx$60-μs T_2 CPMG protons arise from more mobile collagen methylene, such as side chain positions and the amorphous domains between crystalline regions. While previous cortical bone studies have not distinguished these two signal components, a study of dentin—a bone-like material—found two FID components with $T_2^* \approx$12 and 60 μs (32).

In contrast to the signal that survives D_2O, the signal that washes out during D_2O immersion must be a combination of water and non-water exchangeable protons (NWEPs, i.e., exchangeable protons that are not found on water). NWEPs in HCB arise chiefly from amides/hydroxides in collagen and hydroxides in bone minerals, and NWEP abundance can be estimated as follows: assuming that HCB collagen, on average, can be represented by the well-studied model sequences poly(Gly Pro-Pro) (33) and poly(Pro-Hyp-Gly) (34), only 6–12% of collagen protons are exchangeable with D_2O, representing 0.4–0.75% of total collagen mass. Given that 1 mL of HCB contains an average of 0.48 g organic content (35)—greater than 90% of which is collagen (15)—the expected concentration of exchangeable collagen protons in bone is on the order of 1.7–3.2 mol $^1H/L_{bone}$. A similar analysis of bone mineral, using 1.2 g mineral/mL bone (35) and a 0.042% weight fraction of exchangeable hydroxide protons (formulated
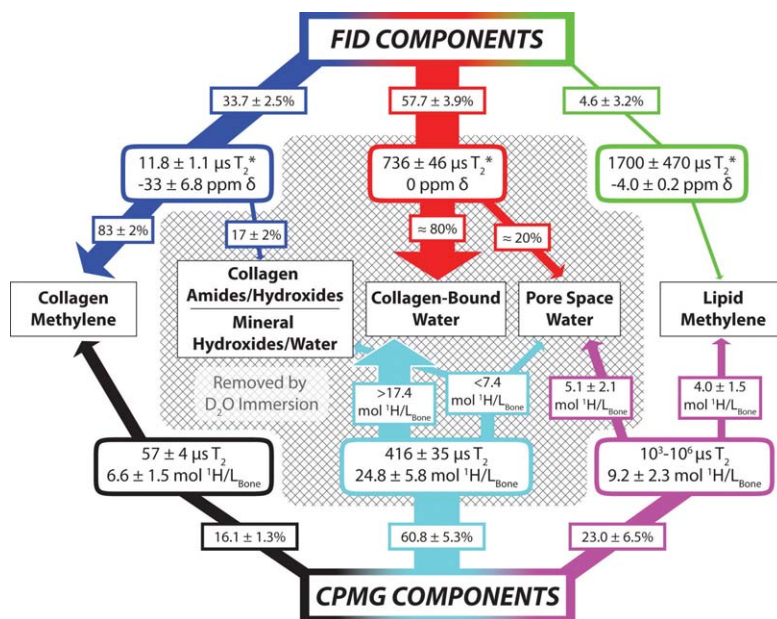
FIG. 6. Postulated biophysical origins of NMR signal relaxation components in HCB. The signal contributions of FID (top) and CPMG (bottom) components to various biophysical proton sources (middle) are indicated by connecting arrows with the same color scheme as in Fig. 5. FID and CPMG signals are first decomposed into three discrete T_2^* and T_2 relaxation components, respectively, with relevant parameters shown in rounded rectangles. Via D_2O immersion studies and two-dimensional exchange spectroscopy experiments, these relaxation components can then be assigned to specific proton sources (see Discussion). All components removed by D_2O immersion are enclosed in the shaded area. If a component arises from more than one proton source, the pendant arrows transect approximate signal fractions (%) or proton concentrations (mol ^{1}H/L_{bone}) to indicate the component's distribution among sources. Arrow widths are proportional to component sizes.

from Cho et al. (36)), gives an expected concentration of 0.5 mol ^{1}H/L_{bone}. Thus, collagen and mineral sources together give a total NWEP abundance of approximately 2–4 mol ^{1}H/L_{bone}. Since NWEPs originate from rather immobile proton sites and are expected to be fast relaxing, it is likely that the fraction of the broadband FID component removed by D_2O ($\approx6\%$ of the total FID signal) accounts for the entire NWEP population. However, it is possible that some of the NWEPs may contribute to the longer-lived FID and CPMG spectral components, but given that an average of 29.5 $\pm$ 7.2 mol ^{1}H/L_{bone} signal was removed from CPMG spectra, we can conclude that this longer-lived signal is predominantly water. Unlike NWEPs, the so-called crystal water protons—ultra-fast-relaxing water in HCB mineral crystal lattice vacancies (37)—must be confined to the small fraction of the broadband FID component removed by D_2O, although the relative contributions of NWEPS and crystal water to this broadband fraction cannot be determined from the measurements herein. With this interpretation, the range of water volume fractions (assuming 1 g/mL water density) found in our six HCB specimens was 17.3–35.6%, which is similar to that found from a cohort of pre- and postmenopausal volunteers and renal osteodystrophy patients (12).

The water signal can be further decomposed into two subpopulations: collagen-bound water (again, collagen being the predominant macromolecule) and relatively free water in porous spaces. Based on μCT at 6-μm isotropic resolution, Haversian canal porosity of the HCB specimens in this study was 4.0 $\pm$ 1.0%, and we estimate a similar volume of lacunar-canalicular pores (14),

making the total average pore volume of the samples $\approx8\%$, or ≈9 mol ^{1}H/L_{bone}. We expect the pore water to have a longer T_2 than the bound water, and $\approx1/2$ of estimated pore water volume can be accounted for by the 5.1 $\pm$ 2.2 mol ^{1}H/L_{bone} that washed out of the long-T_2 component. The remaining pore water may be included in the ≈400 μs T_2 CPMG component (accounting for no more than $\approx15\%$ of it) and/or some of this water may have been wicked inadvertently from the larger pores during sample handling. Thus, including possible contributions of both NWEPs and porous water, the remainder of the ≈400 μs T_2 CPMG component must be *at least* $\approx70\%$ collagen-bound water (or 17.4–24.8 mol ^{1}H/L_{bone}). This assignment is roughly consistent with literature estimates of 0.48 g collagen per mL of HCB (35) and 0.49 g water bound per gram collagen in bone, which together equate to an expected bound-water proton concentration of ≈26 mol ^{1}H/L_{bone}.

The assignments of the ≈60-μs and ≈400-μs components to collagen methylene protons and collagen-bound water, respectively, are also consistent with the observation of exchange between these components seen in our RESXY measurements (Fig. 4). Interestingly, the observation that REXSY demonstrates exchange between these two components but only the ≈400-μs T_2 component is removed by D_2O indicates that the observed magnetization exchange is mediated by a through-space, dipole-dipole interaction, rather than chemical exchange, which further supports our biophysical assignments. It also is noteworthy that our biophysical assignments in HCB are similar to previous findings in human dentin (32) (determined through ^{1}H NMR relaxometry and sample

dehydration), with one particular exception: the $\approx$60-μs decay component in dentin was attributed to a mixture of hydroxide and water, in addition to protein. At least one other study has identified very-short-lived water in bone mineral (37); however, it disappeared with dehydration and so we presume it would be washed out with D_2O. Herein, we conclude that the 60-μs T_2 component is predominantly protein derived because it survives D_2O immersion.

Finally, it should be noted that the broad age range of the HCB donors herein allowed the study of common relaxation features across presumably diverse physiologic states. Interestingly, relaxation rates among all the donors were similar, indicating that the chemical nature of various bone proton milieux persist during aging. The dominant source of variability observed among donors was in the relaxation component pool sizes; for example, the oldest and most visibly osteoporotic donor had a larger long-lived T_2 component (Fig. 2c, turquoise line) than the other donors. However, a thorough analysis of the interdonor relaxation differences would require a significantly larger number of donors, which is beyond the scope of this work but is the subject of future study.

CONCLUSIONS

In summary, ^1H NMR signal from HCB was found to exhibit a broad distribution of transverse relaxation components attributable to known bone proton sources (Fig. 6) as follows: i) $T_2^* \approx$12 μs, derived $\approx$80% from collagen backbone methylene protons and the remainder from NWEPs (amide/hydroxide) and possibly adsorbed mineral water, ii) $T_2 \approx$60 μs, derived predominantly from collagen side-chain or otherwise mobile methylene protons, iii) $T_2 \approx$400 μs, derived predominantly from water bound to the collagen responsible for the 12-μs T_2^* and 60-μs T_2 components, iv) $T_2 \approx$milliseconds-second, derived $\approx$60% from pore water and $\approx$40% from lipid methylene protons. These findings indicate that modern ultrashort echo time MRI of cortical bone is dominated by signal from water bound to bone matrix collagen and that commonly used long-T_2 suppression techniques for enhancing bone contrast will suppress signal from lipids and pore space water that may be of biological/clinical interest. Also, while some short-T_2 signals in HCB may be difficult to quantify directly, the interaction between their underlying proton pool and the dominant water signal offers the potential to probe prohibitively fast-relaxing HCB signals through magnetization transfer contrast. Finally, there was considerable variability in the lipid and pore water content across the diverse (albeit small number of) HCB samples studied herein, indicating these two metrics may contain the useful information on bone quality and health.

REFERENCES

1. Johnell O, Kanis JA, Oden A, Johansson H, De Laet C, Delmas P, Eisman JA, Fujiwara S, Kroger H, Mellstrom D, Meunier PJ, Melton LJ, O'Neill T, Pols H, Reeve J, Silman A, Tenenhouse A. Predictive value of BMD for hip and other fractures. J Bone Miner Res 2005;20:1185–1194.

2. Bembey AK, Bushby AJ, Boyde A, Ferguson VL, Oyen ML. Hydration effects on the micro-mechanical properties of bone. J Mater Res 2006;21:1962–1968.

3. Nyman JS, Roy A, Shen XM, Acuna RL, Tyler JH, Wang XD. The influence of water removal on the strength and toughness of cortical bone. J Biomech 2006;39:931–938.

4. Yan JH, Daga A, Kumar R, Mecholsky JJ. Fracture toughness and work of fracture of hydrated, dehydrated, and ashed bovine bone. J Biomech 2008;41:1929–1936.

5. Sasaki N, Enyo A. Viscoelastic properties of bone as a function of water-content. J Biomech 1995;28:809–815.

6. Fernandez-Seara MA, Wehrli SL, Takahashi M, Wehrli FW. Water content measured by proton-deuteron exchange NMR predicts bone mineral density and mechanical properties. J Bone Miner Res 2004;19:289–296.

7. Bembey AK, Oyen ML, Bushby AJ, Boyde A. Viscoelastic properties of bone as a function of hydration state determined by nanoindentation. Philos Mag 2006;86:5691–5703.

8. Nyman JS, Ni QW, Nicolella DP, Wang XD. Measurements of mobile and bound water by nuclear magnetic resonance correlate with mechanical properties of bone. Bone 2008;42:193–199.

9. Balcom BJ, MacGregor RP, Beyea SD, Green DP, Armstrong RL, Bremner TW. Single-point ramped imaging with T-1 enhancement (SPRITE). J Magn Reson Ser A 1996;123:131–134.

10. Idiyatullin D, Corum C, Park JY, Garwood M. Fast and quiet MRI using a swept radiofrequency. J Magn Reson 2006;181:342–349.

11. Gatehouse PD, Bydder GM. Magnetic resonance imaging of short T-2 components in tissue. Clin Radiol 2003;58:1–19.

12. Techawiboonwong A, Song HK, Leonard MB, Wehrli FW. Cortical bone water: in vivo quantification with ultrashort echo-time MR imaging. Radiology 2008;248:824–833.

13. Olszta MJ, Cheng XG, Jee SS, Kumar R, Kim YY, Kaufman MJ, Douglas EP, Gower LB. Bone structure and formation: a new perspective. Mater Sci Eng R 2007;58:77–116.

14. Cowin SC. Bone poroelasticity. J Biomech 1999;32:217–238.

15. Weiner S, Wagner HD. The material bone: structure mechanical function relations. Annu Rev Mater Sci 1998;28:271–298.

16. Meiboom S, Gill D. Modified spin-echo method for measuring nuclear relaxation times. Rev Sci Instrum 1958;29:688–691.

17. Callaghan PT, Arns CH, Galvosas P, Hunter MW, Qiao Y, Washburn KE. Recent Fourier and Laplace perspectives for multidimensional NMR in porous media. Magn Reson Imaging 2007;25:441–444.

18. English AE, Whittall KP, Joy MLG, Henkelman RM. Quantitative 2-dimensional time correlation relaxometry. Magn Reson Med 1991;22:425–434.

19. Dortch RD, Horch RA, Does MD. Development, simulation, and validation of NMR relaxation-based exchange measurements. J Chem Phys 2009;131:11.

20. Whittall KP, Mackay AL. Quantitative interpretation of NMR relaxation data. J Magn Reson 1989;84:134–152.

21. Venkataramanan L, Song YQ, Hurlimann MD. Solving Fredholm integrals of the first kind with tensor product structure in 2 and 2.5 dimensions. IEEE Trans Signal Process 2002;50:1017–1026.

22. Edzes HT, Samulski ET. Measurement of cross-relaxation effects in proton NMR spin-lattice relaxation of water in biological-systems-hydrated collagen and muscle. J Magn Reson 1978;31:207–229.

23. Macura S, Huang Y, Suter D, Ernst RR. Two-dimensional chemical-exchange and cross-relaxation spectroscopy of coupled nuclear spins. J Magn Reson 1981;43:259–281.

24. Turov VV, Gun'ko VM, Zarko VI, Leboda R, Jablonski M, Gorzelak M, Jagiello-Wojtowicz E. Weakly and strongly associated nonfreezable water bound in bones. Colloids Surf B 2006;48:167–175.

25. Fantazzini P, Brown RJS, Borgia GC. Bone tissue and porous media: common features and differences studied by NMR relaxation. Magn Reson Imaging 2003;21:227–234.

26. Ong HH, Wehrli SL, Wehrli FW. Proton NMR study of transverse relaxation in rabbit and rat cortical bone. J Bone Miner Res 2008;23:S494.

27. Ni QW, King JD, Wang XD. The characterization of human compact bone structure changes by low-field nuclear magnetic resonance. Meas Sci Technol 2004;15:58–66.

28. Wang XD, Ni QW. Determination of cortical bone porosity and pore size distribution using a low field pulsed NMR approach. J Orthop Res 2003;21:312–319.

29. Ni QW, Santos ADL, Lam H, Qin YX. Assessment of simulated and functional disuse on cortical bone by nuclear magnetic resonance. Adv Space Res 2007;40:1703–1710.

30. Ni QW, Nicolella DP. The characterization of human cortical bone microdamage by nuclear magnetic resonance. Meas Sci Technol 2005; 16:659–668.

31. Ni QW, Nyman JS, Wang XD, De Los Santos A, Nicolella DP. Assessment of water distribution changes in human cortical bone by nuclear magnetic resonance. Meas Sci Technol 2007;18:715–723.

32. Schreiner LJ, Cameron IG, Funduk N, Miljkovic L, Pintar MM, Kydon DN. Proton NMR spin grouping and exchange in dentin. Biophys J 1991;59:629–639.

33. Boryskina OP, Bolbukh TV, Seminenov MA, Gasan AI, Maleev VY. Energies of peptide-peptide and peptide-water hydrogen bonds in collagen: evidences from infrared spectroscopy, quartz piezogravimetry and differential scanning calorimetry. J Mol Struct 2007;827:1–10.

34. Berisio R, Vitagliano L, Mazzarella L, Zagari A. Crystal structure of a collagen-like polypeptide with repeating sequence Pro-Hyp-Gly at 1.4 angstrom resolution: implications for collagen hydration. Biopolymers 2000;56:8–13.

35. Gong JK, Arnold JS, Cohn SH. Composition of trabecular and cortical bone. Anat Rec 1964;149:325–331.

36. Cho G, Wu Y, Ackerman JL. Detection of hydroxyl ions in bone mineral by solid-state NMR spectroscopy. Science 2003;300: 1123–1127.

37. Wilson EE, Awonusi A, Morris MD, Kohn DH, Tecklenburg MMJ, Beck LW. Three structural roles for water in bone observed by solid-state NMR. Biophys J 2006;90:3722–3731.